Biosensors and Bioelectronics 298 (2026) 118345

Contents lists available at ScienceDirect

Biosensors and Bioelectronics

journal homepage: www.elsevier.com/locate/bios

A stretchable continuous glucose monitor for skin-conformable wound management

Binbin Cui [1], Ivo Pang [1], Shilei Dai, Xiaonan Chen, Dingyao Liu, Xinyu Tian, Wensheng Lin, Jing Bai, Xinran Zhang, Shiming Zhang [*]

Department of Electrical and Electronic Engineering, The University of Hong Kong, Hong Kong Special Administrative Region of China

A B S T R A C T

Chronic wounds, especially those linked to diabetes, require continuous monitoring and timely interventions to prevent severe complications. The emergence of smart bandages equipped with multifunctional sensors offers a promising avenue to alleviate the burden on healthcare systems while minimizing delays in medical care. However, conventional electrochemical sensors often face limitations, including inadequate detection sensitivity and poor mechanical compatibility with biological tissue, thereby restricting their utility in smart bandages for long-term wound care applications. In this study, we present a stretchable continuous glucose monitor (CGM), based on organic electrochemical transistors (OECTs), for chronic wound care. By leveraging the amplification capability and the mechanical properties of stretchable OECTs, this platform achieves both high sensitivity and tissue compatibility. To demonstrate the potential for practical use, the sensors are integrated into a compact, coin-sized wearable readout system, enabling continuous and comfortable wound monitoring.

1. Introduction

Skin wound healing is a highly intricate physiological process that encompasses a multitude of biochemical processes and four overlapping phases: hemostasis, inflammation, proliferation, and remodeling (Liang et al., 2021; Luo et al., 2021). Each stage of wound healing is crucial and must be executed with precision for the skin to re-establish its integrity. If not treated properly, or in the presence of health conditions such as aging, diabetes, or vascular diseases, even a small wound can develop into a chronic wound, which may remain unhealed for years (Derakhshandeh et al., 2018; Heck et al., 2023).

Proper wound condition monitoring is essential for identifying changes in physiological signals and initiating timely medical intervention (Dong and Guo, 2021; Farahani and Shafiee, 2021; McLister et al., 2016). Smart bandages are a promising wearable platform for chronic wound care, utilizing hydrogel dressings to cover wounds and sensors to detect physiological indicators such as pH (Farooqui and Shamim, 2016; Mirani et al., 2017; Salvo et al., 2017), temperature (Hattori et al., 2014; Salvo et al., 2017), oxygenation (Mostafalu et al., 2015), and glucose levels at the wound site (Liu et al., 2022b). These bandages can serve as point-of-care technology by using intelligent systems to monitor the wound environment without requiring patients to visit medical facilities.

However, most smart bandage sensors rely on traditional electrochemical or optical methods, that have limitations in real-time clinical use (Mostafalu et al., 2018; Yang and Gao, 2019). First, traditional electrochemical sensors are relatively unstable due to reference electrode degradation over time (Lim et al., 2020). Second, their passive sensing nature results in low sensitivity, making them unsuitable for early diagnosis of wound complications (Shirzaei Sani et al., 2023; Wang et al., 2022). Third, the mechanical compatibility between these sensors and soft, dynamic tissue is poor due to the inherent rigidity of the materials, causing discomfort and potential device failure during long-term use (Li et al., 2019; Oh et al., 2018).

Organic electrochemical transistors (OECTs), as high signal-to-noise-ratio bioelectronic devices, have been extensively investigated and designed as low-voltage and highly sensitive sensing platforms for detecting various chemical and biological analytes (Bai et al., 2022; Ji et al., 2016; Marks et al., 2022). Organic mixed ionic–electronic conductors (OMIECs), such as poly (3,4-ethylenedioxythiophene) polystyrene sulfonate (PEDOT:PSS), are commonly used as the redox-active channel material of OECTs, enabling both electron and ion transport (Zhang and Cicoira, 2017; Zhang et al., 2019). By controlling the polarity and amplitude of gate voltage, the channel conductivity of OECTs can be effectively modulated via in situ volumetric ionic doping/de-doping processes. OECTs provide high sensitivity and low operating voltage (<1 V) because they employ the entire volume of OMIECs as the effective channel, leading to a substantial volumetric

* Corresponding author.
E-mail address: beszhang@hku.hk (S. Zhang).
[1] These authors contributed equally to this work.

https://doi.org/10.1016/j.bios.2025.118345
Received 18 August 2025; Received in revised form 12 December 2025; Accepted 26 December 2025
Available online 27 December 2025

capacitance, a low impedance, and a high transconductance (Liu et al., 2024; Pappa et al., 2018; Zhang et al., 2017; Liu et al., 2025).

To accurately measure biomarkers in the wound area, sensors must conformably adhere to the skin and maintain stretchability to ensure mechanical stability during skin deformation (Mostafalu et al., 2018; Shirzaei Sani et al., 2023). However, traditional OECT-based sensors are mainly fabricated on rigid or flexible substrates (Ji et al., 2016), thereby failing to meet the mechanical requirements (stretchability and conformability) for wearable chronic wound care.

In this study, we present a stretchable OECT-based glucose sensor integrated onto a double-network hydrogel dressing patch (Fig. 1A). The device demonstrates high sensitivity (>20 μA/mM), long stability (15 days) and excellent stretchability (50% strain), making it ideal for chronic wound care management. We systematically investigated the enzyme distribution on the functional gate electrode during stretching and identified the factor contributing to the device's stable performance under strain. Notably, we achieved integration of our sensor onto the hydrogel dressing with a coin-sized wearable readout system, delivering a fully wearable and conformable smart bandage system (Fig. 1B and C). This system shows a linear response to glucose concentrations between 2 mM and 10 mM, with high sensitivity (>20 μA/mM).

2. Results and discussion

2.1. Fabrication of stretchable OECT-based glucose sensor

The OECT-based devices utilize PEDOT:PSS as both the electrode and channel material, offering several advantages, including high conductivity, excellent stability in aqueous environments, biocompatibility, and cost-effective solution processing (Kayser and Lipomi, 2019). The dual use of PEDOT:PSS for both electrode and channel material not only simplifies device fabrication but also enhances tensile stability.

Traditionally, complex PEDOT:PSS patterns are fabricated using expensive and intricate photolithographic etching techniques (Zhang et al., 2017). In this work, we present a cost-effective and easily implementable additive manufacturing approach by employing inkjet printing to fabricate PEDOT:PSS-based OECT devices (Faddoul et al., 2014; Teichler et al., 2013). Commercially available PEDOT:PSS ink, compatible with inkjet printing, was optimized to achieve a uniform and conductive layer on a soft substrate (Fig. 1D). Additionally, the inkjet-printed electrodes (pre-stretched) demonstrated excellent stretchability under 50% strain (Fig. S1).

For device fabrication, thermoplastic polyurethane (TPU) was chosen as the substrate due to its ability to provide OECTs with a high current on/off ratio by reducing oxygen permeability (PO_2) (Liu et al., 2022a). Fig. 2A illustrates the fabrication process of the PEDOT:PSS pattern on the TPU substrate using inkjet printing. To enhance the operational stability of the device and minimize leakage current, TPU encapsulant paste was used for the insulation layer by screen printing technology.

Fig. 2B and D presents the representative transfer, transconductance, and output curves of the OECT device. The OECTs exhibited a transconductance of 0.8 mS and stable electrical performance over 50 cycles (Fig. 2C). Furthermore, our OECT device maintained consistent performance under 50% strain (Fig. 2E). To evaluate the reproducibility of the fabricated OECTs, we fabricated and characterized six separate samples and tested them under identical conditions. The overlay of their transfer curves in Fig. S2 demonstrates consistent transistor behavior and excellent reproducibility. Furthermore, the long-term stability of the device was measured by observing the current drift over 600 s under a constant applied gate voltage (Fig. S3). The results exhibited minimal drifting during this period, confirming the long-term stability of the device.

Conventional glucose sensors based on metal electrodes typically employ enzymes to catalyze glucose, leading to the generation of hydrogen peroxide (Ji et al., 2016). The metal electrode then catalyzes hydrogen peroxide, inducing current changes in the electrode (Teymourian et al., 2020; Wang, 2008). While effective in glucose sensing, these rigid metal-based devices are limited in applications requiring flexibility. In comparison, our OECTs offer superior stretchability and conformability, making them well-suited for epidermal biosensing. To realize OECT-based biosensors, the gate electrode can be modified with mediators such as ferrocene (Fc) derivatives and ferricyanides (Teymourian et al., 2020) to facilitate electron transfer from enzyme reactions to the gate electrode. In this study, we utilized Fc as the mediator (Bihar et al., 2018), widely recognized for glucose sensing applications, and introduced a biocompatible chitosan membrane layer to confine the enzyme and mediator, thus enhancing the sensor's stability.

The gate electrode was fabricated using inkjet printing technology. A

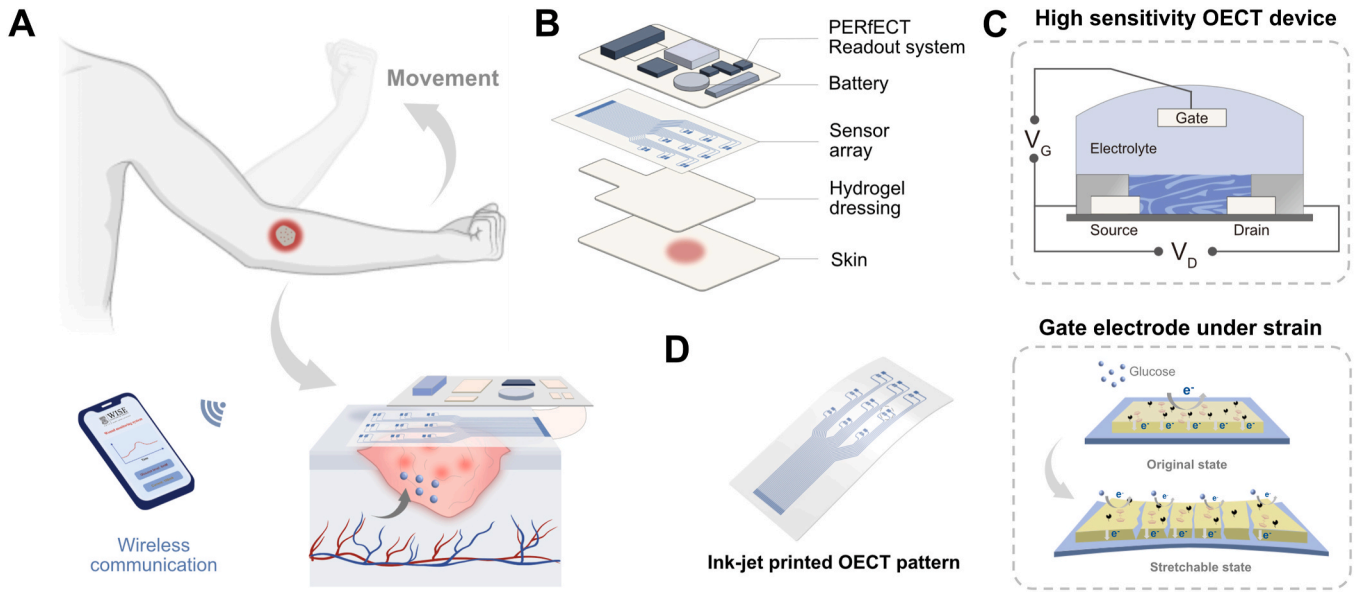

Fig. 1. The schematic of smart wound monitoring system. (A) The smart bandage system for wound glucose monitoring. **(B)** An exploded view of the wound monitoring system, showcasing its key components, including the hydrogel dressing layer, stretchable sensor array, and the wearable readout system. **(C)** A schematic representation of the OECT device structure. **(D)** A schematic representation of the stretchable glucose sensor array and the working mechanism under strains.

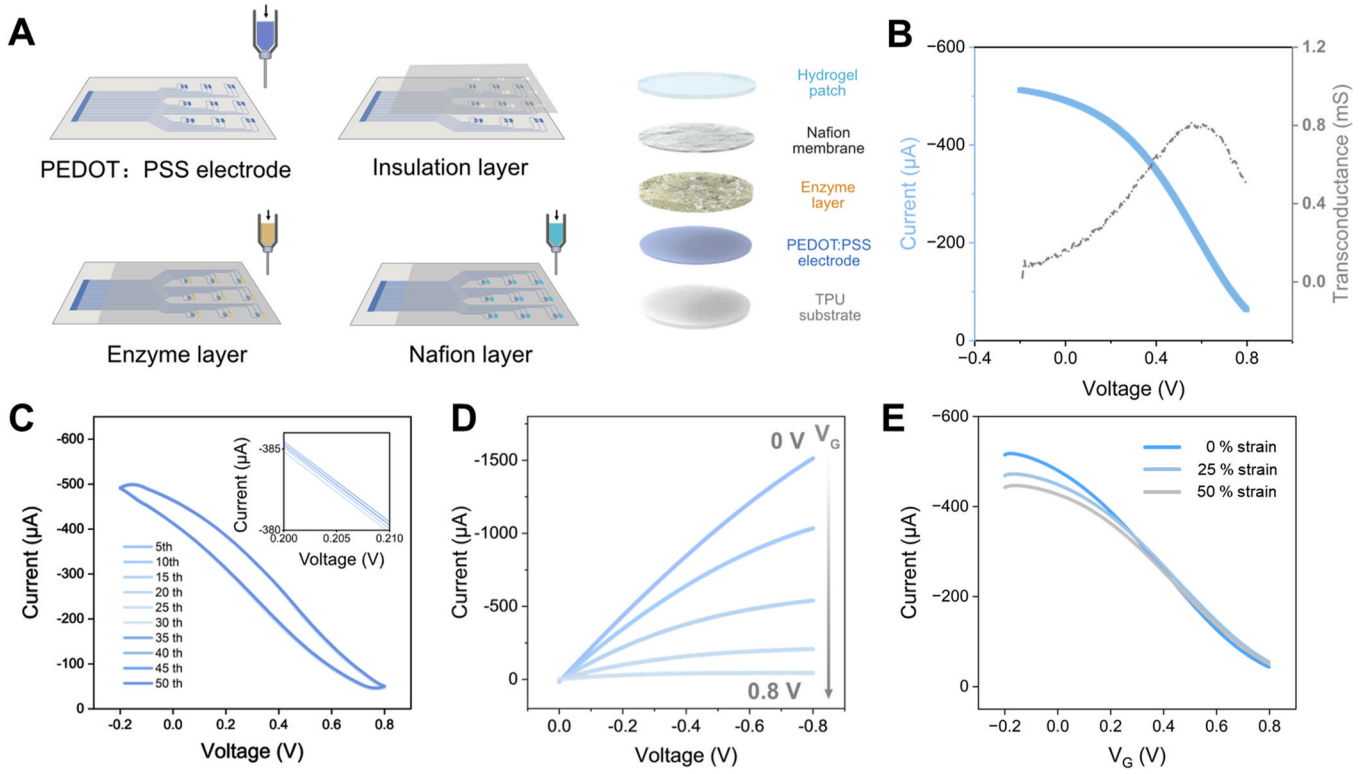

Fig. 2. The fabrication of stretchable OECT devices. (A) Fabrication process of stretchable OECT sensors, including electrode pattern, insulation layer, enzyme layer and hydrogel layer. **(B)** The transfer curve and the transconductance curve of stretchable OECT. The gate voltage is from −0.2 V to 0.8 V and the channel voltage was fixed at −0.2 V. **(C)** The stability performance of the stretchable OECTs and the inset shows a zoomed-in plot of the transfer curve. **(D)** The output curve of stretchable OECT sensors. The gate voltage (V_G) ranges from 0 V to 0.8 V. **(E)** The transfer curve tested under different strains (0–50%). The gate voltage is from −0.2 V to 0.8 V and the channel voltage is fixed at −0.2 V.

chitosan-enzyme solution was printed onto the gate electrode, followed by a Nafion membrane layer, which served as an anti-interference barrier to block electroactive interferents such as ascorbic acid (AA), dopamine (DA) and uric acid (UA). After modification, the double-layer capacitance of the functionalized gate electrode increased, which indicated that the enzyme layer was immobilized (Fig. S4).

2.2. Sensing performance of the OECT device

The enzymatic sensing mechanism of the OECT-based glucose sensor is illustrated in Fig. 3A. In the absence of glucose (solid line), the electrolyte potential is determined by the relative capacitances at the gate electrode and channel interfaces. In the presence of glucose (dashed line), the electrolyte potential rises in accordance with the Nernst equation. This increase in potential leads to a rise in the effective gate voltage (red dashed line) due to Faradaic effects, which modulate the channel current as described by Equation (1).

$$V_G^{eff} = V_G + (1+\gamma)\frac{kT}{2e}\ln[Glu] + constant^* \quad (1)$$

Where κ is the Boltzmann constant, T is the temperature, and γ is the ratio between the capacitance of the two interfaces: electrolyte/channel interface (C_{CE}) and electrolyte/gate interface (C_{GE}), $\gamma = C_{CE}/C_{GE}$. This constant contains details of proton and oxygen concentrations and the formal potential (Bernards et al., 2008; Shim et al., 2009).

We evaluated the sensing performance of a three-electrode electrochemical (EC) device, which serves as a reference for comparing the performance of our OECT-based biosensor. The working electrode of the EC device consists of a PEDOT:PSS thin film coated on a TPU substrate, modified with the same enzyme using the previously described method (electrode area: 0.16 cm^2). Scanning electron microscope (SEM) images of the modified electrode are presented in Fig. S5. The three-electrode EC setup was completed with a platinum plate serving as the counter electrode, and an Ag/AgCl electrode as the reference electrode. To determine the optimal operating potential for EC glucose sensing, cyclic voltammetry (CV) curves of the PEDOT:PSS-based EC device were measured in phosphate-buffered saline (PBS, pH 7.4). The bio-functionalized PEDOT:PSS exhibited well-defined and symmetric peaks at approximately 0.2 V (anodic) and 0.15 V (cathodic), which are the characteristic CV peaks of Fc (Fig. S6).

To evaluate the EC sensor performance, we monitored the real-time changes in sensor current during the stepwise addition of glucose to the measurement solution (from 1 mM to 8 mM). Based on the characteristic anodic CV peaks, we chose 0.2 V as the working voltage and then tested the amperometric curve for the successive addition of glucose to the PBS solution (Fig. S6). The EC device showed a linear calibration curve between 1 and 8 mM (obtained from the current density according to glucose concentration). The sensitivity of the EC device is estimated to be 2.53 μA/mM based on a linear least-squares fitting of the calibration data.

To characterize the sensing performance of our OECT-based device, we measured the current response of our device to different glucose concentrations, establishing a broad responsive range from as low as 10^{-3} mM–10^2 mM glucose concentrations (Fig. S7). To demonstrate the potential of our device in practical use, we calibrated the current responsiveness of our device to 2–10 mM glucose, which covers the normal glucose level range of a normal adult. As shown in Fig. 3B, our devices exhibit good detection ability for blood glucose concentrations of 2–10 mM. From the calibrated response curve (Fig. 3C), a sensitivity of 21 μA/mM was achieved, which is about 8 times higher than that achieved with the PEDOT:PSS-based EC device. To further assess the selectivity of the OECT-based glucose sensor, we tested its response to 2

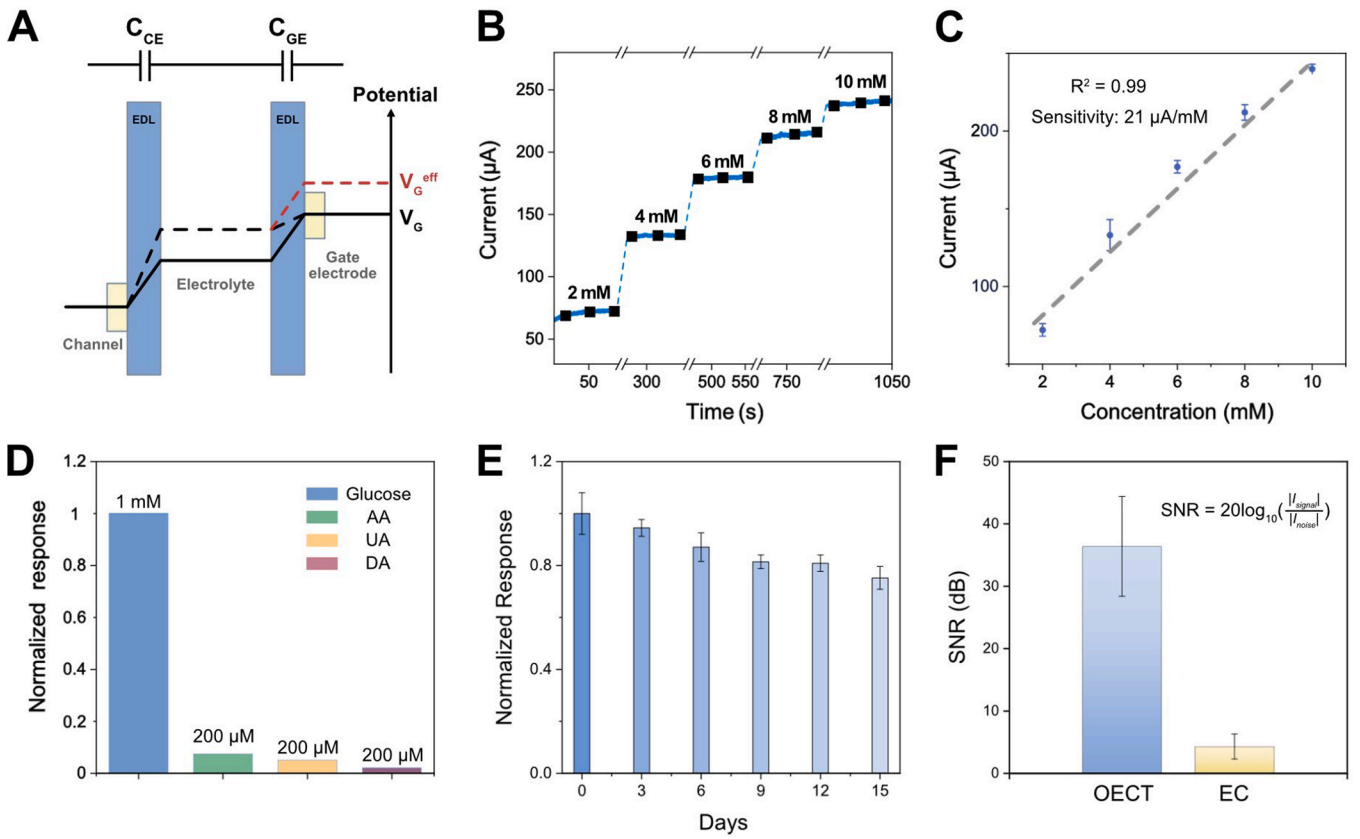

Fig. 3. Sensing performance of stretchable glucose sensor. (A) The potential change between the working and counter electrodes (gate electrode and channel). **(B)** ΔI_D current response change in the range of 2–10 mM. **(C)** The calibration curve of the glucose sensor. **(D)** Anti-interference detection of OECT-based glucose sensor. In the interference tests, the concentrations of these compounds in PBS solution were 200 μM for ascorbic acid, 200 μM for uric acid, and 200 μM for dopamine, and 1 mM for glucose. **(E)** Stability of stretchable glucose sensor over 15 days. All the devices were tested at fixed biases: $V_D = -0.4$ V and $V_G = 0.2$ V. The normalized response refers to the device sensitivity across glucose concentration range of 2–10 mM. **(F)** SNR comparison of the OECT sensor and the EC sensor. SNRs for both OECT and EC were calculated through the equation indicated in the inset of the figure.

mM glucose in the presence of an interference agent, 200 μM AA, DA, UA. As shown in Fig. 3D, the response current remained largely unchanged after the addition of the interference agent.

To evaluate the shelf life of the devices, we tested the performance of glucose sensors stored for 1–15 days after fabrication. Our OECT-based stretchable glucose sensordemonstrated stable performance after 15 days of storage, as shown in Fig. 3E. Although slight deterioration was observed over long-term storage, the sensitivity remained sufficiently high for practical use, retaining 75 ± 2 % of the normalized response (NR) recorded on the first day. Additionally, we compared the current response of the sensor with that of an EC sensor (Fig. S8). The sensor exhibited a higher signal-to-noise ratio (SNR) than the EC sensor (Fig. 3F).

2.3. Stretchability of the OECT device

Fig. 4A shows the schematic of the stretchable gate electrode during working condition. After repeated stretches, the enzymatic electrode maintained its performance. To assess this, we conducted tests to determine the electrode resistance change under 50% strains, and found that the electrical property of the PEDOT:PSS thin film electrode remained stable for over 100 strain cycles (Fig. S1). We also compared optical microscopic images of PEDOT:PSS films under different strain values and observed that PEDOT:PSS films on TPU substrates exhibited almost no cracks at 50% strain (Fig. 4B).

To investigate the enzyme-modified electrode under stretching, we observed optical images of the enzyme electrode under different strains. As the chitosan membrane is not stretchable and is approximately 15 μm thick (Fig. S5), cracks appeared on the enzyme electrode membrane during the stretching process, as shown in Fig. 4B. However, it should be noted that due to the viscosity of chitosan, the membrane did not detach from the substrate, and the enzyme remained entrapped in the enzyme layer. To determine the enzyme distribution, we utilized FITC (fluorescein isothiocyanate) (Paul et al., 2023), which is a common fluorescein material for enzyme labeling, to label the enzyme cluster and then modify the gate electrode. We compared the enzyme cluster distribution in fluorescence microscopy images of the enzyme electrode under different strain values and observed that the enzyme cluster distribution remained nearly unchanged under 50% strain, as illustrated in Fig. 4C. Subsequently, we evaluated the glucose-sensing property of the OECT under different strains, as shown in Fig. 4B. The calibration curve of the glucose sensor demonstrates that sensitivity did not decrease substantially under stretching.

2.4. Fabrication of wound monitoring system

This smart bandage system comprises three key components: a stretchable glucose sensor, a hydrogel dressing, and the PERfECT (Personalized Electronic Reader for Electrochemical Transistor) readout system (Tian et al., 2022). The stretchable OECT-based glucose sensor is integrated into a hydrogel dressing to enable continuous in-situ monitoring of wound glucose directly on rats (Fig. 5A). The PERfECT readout system is a wearable, ultra-lightweight, coin-sized device that allows real-time monitoring of glucose levels in wounds, ensuring patient comfort (Tian et al., 2022) (Fig. S9). We also use a PAAm/NaAlg (polyacrylamide/sodium alginate) double-network hydrogel as the dressing

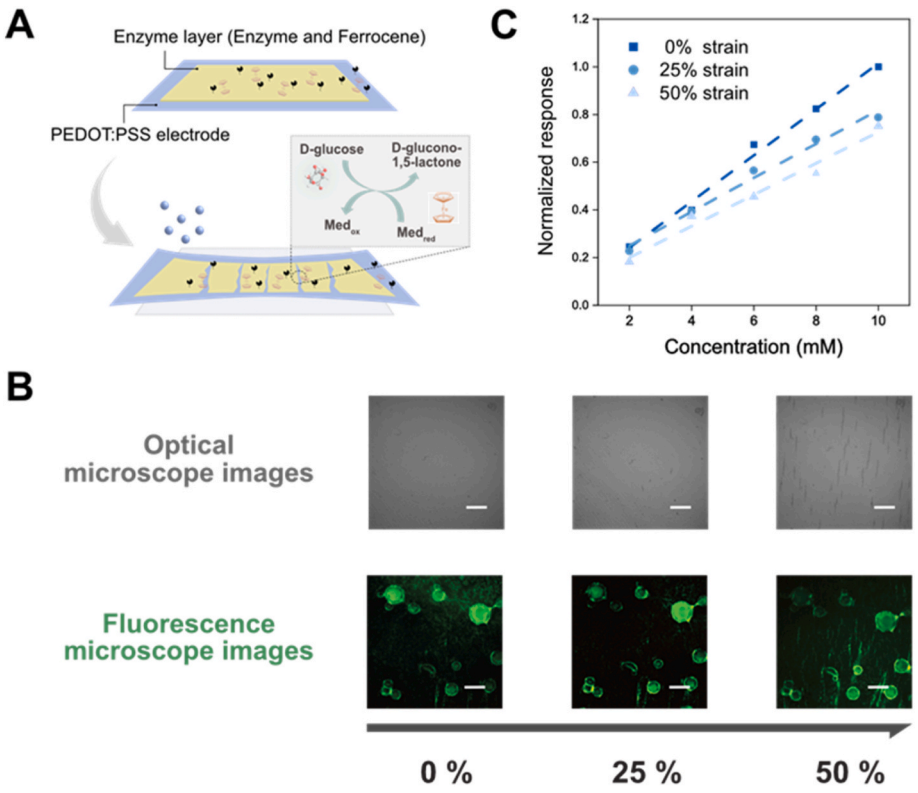

Fig. 4. Stretchability of the OECT device. (A) The schematic of the enzyme distribution on the gate electrode during stretching, along with **(B)** optical microscope and fluorescence microscope images of the modified PEDOT:PSS electrode. **(C)** Corresponding calibration plot of OECT devices (current vs. concentration) under different strains. The V_G is fixed at 0.2 V, and V_D is fixed at −0.4 V.

patch (Sun et al., 2012).

The device's temporal electrochemical signal, recorded with incremental glucose additions, is shown in Fig. 5B. Before testing, the mice were fasted for 24 h to stabilize their blood glucose levels. Under anesthesia, a 400 mM glucose solution in Dulbecco's Phosphate Buffer (DBPS) (adjusted based on body weight) was administered to the mice via a syringe (Bai et al., 2024; Cheng et al., 2022). The results indicated a linear response to glucose concentrations ranging from 2 to 10 mM, aligning with physiological levels. The wearable smart bandage demonstrated commendable stability, achieving a sensitivity of 22.2 μA/mM, as demonstrated in Fig. 5B and C.

3. Conclusion

In summary, we presented a stretchable CGMs based on OECTs for wound care monitoring. This sensor can detect glucose levels in the 2–10 mM range while maintaining stable performance under 50% strain. We employed inkjet printing for sensor fabrication, reducing production costs and streamlining the process. We investigated the mechanisms of the sensor's stability under stretch, identifying the structural integrity of stretchable electrodes and consistent enzyme distribution as key contributors to its robustness. Our work highlights the potential of OECT devices as promising sensing components for assembling smart bandages, paving the way for future tissue-integratable bioelectronics applications.

4. Materials and method

4.1. Reagents and apparatus

PEDOT:PSS aqueous suspension (Clevios PH1000) was purchased from Heraeus Electronics Materials. Glycerol, dodecylbenzene sulfonic acid (DBSA), (3-glycidyloxypropyl) trimethoxy silane (GOPS), acrylamide (AAm), sodium alginate (SA), N,N′-Methylenebisacrylamide (MBAA), and ammonium persulphate (APS) were purchased from Sigma-Aldrich Co. The thermoplastic polyurethane (TPU) film was purchased from 3M Co.. TPU encapsulation paste (Elec-LT506) was purchased from Shenzhen Yilai Technology Co., Ltd.. The D-(+)-Glucose (>99.5 % (GC)), ascorbic acid (≥99 %), uric acid, dopamine, phosphate-buffered saline (pH 7.2–7.5), and Nafion (5 wt% in a mixture of lower aliphatic alcohols and water) were purchased from Aladdin Co.. Ferrocene (99 %), and glucose oxidase (GOx, >180 U/mg) were purchased from Macklin Co.. Chitosan (200–600 mPa s) was purchased from TCL. Acetic acid was bought from Alfa Aesar Co. The FITC conjugation kit was purchased from Sangon Biotech Co., Ltd.

All electrical characterizations were conducted using phosphate-buffered saline (PBS) solution as the electrolyte. A CHI660E electrochemical workstation (CH Instruments, Inc.) was employed to analyze the electrochemical properties of various gate electrodes. The strain tests on the film and hydrogel were performed using a tensile testing machine. For transistor characterizations, the transfer, output, and transient responses were measured with a Keysight B2902 source-measure unit controlled by Quick IV software. The cracking of the PEDOT:PSS film under strain and the enzyme distribution were examined using a Nikon optical/fluorescence microscope.

4.2. Inkjet printing for OECT device

The PEDOT:PSS aqueous suspension was initially stirred for 3 min and then mixed with glycerol (5 v/v%) and DBSA (0.1 v/v%) using a vortex mixer (MX-S). Glycerol was added to enhance film conductivity, while DBSA improved the wetting properties of the films on substrates. The mixed suspension was then filtered using a polytetrafluoroethylene (PTFE) membrane (0.22 μm pore size) to remove aggregates. A SW3060 inkjet printer (Yiwu Yangtian Electronic Technology Co., Ltd) was used

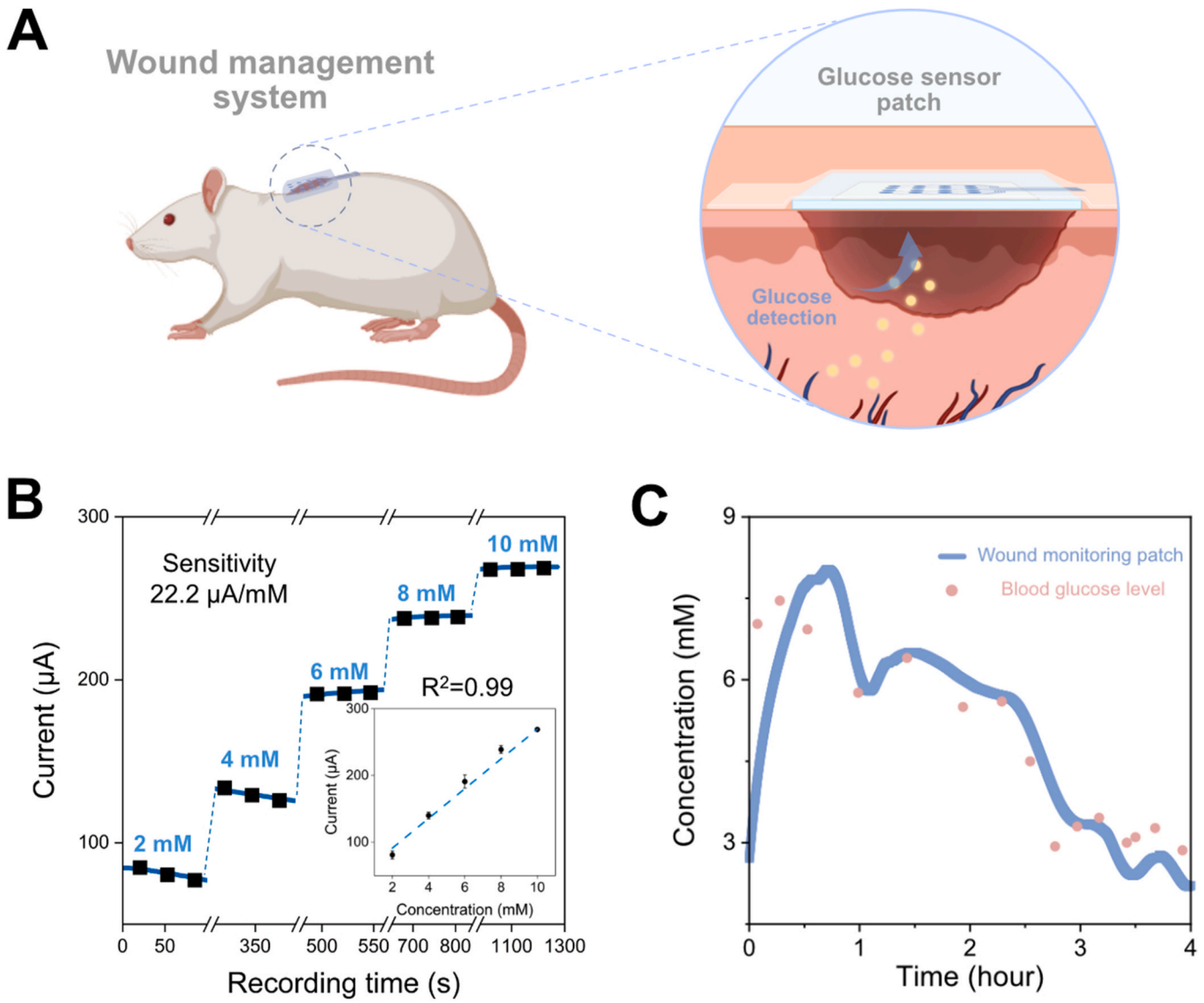

Fig. 5. Continuous wound glucose monitoring on rat. (A) The schematic of the smart bandage system with stretchable OECT sensors. **(B)** Real-time glucose monitoring using a PERfECT readout device. The V_G is set at 0.2 V, and the V_D at −0.4 V. The sensitivity was around 22.2 μA/mM and the inset figure shows good linearity of the concentration with the current. **(C)** In-vivo continuous glucose monitoring with the smart bandage system.

to print the electrodes onto TPU (30 μm thickness). After printing, the sample was heated at 120 °C for 30 min.

4.3. Modifications of the gate electrode

GOx (30 mg) was dissolved in 1 mL of PBS solution with magnetic stirring at 1000 rpm for 1 h. Meanwhile, 50 mg of chitosan was mixed with 50 μL of acetic acid in 10 mL of deionized water and stirred at 500 rpm for 12 h at 60 °C. Subsequently, 1 mL of the prepared GOx solution was combined with 1 mL of the chitosan solution and sonicated for 20 min prior to use. For the preparation of the ferrocene solution, ferrocene (18.6 mg) was dissolved in 10 mL of ethanol and stirred at 500 rpm for 2 h at room temperature. Following this, 100 μL of the ferrocene solution was mixed with 100 μL of the enzyme solution and inkjet-printed onto the PEDOT:PSS electrode. The electrode was allowed to dry at room temperature for 1 h, and the gate electrode was further dried at 4 °C for 12 h. Finally, Nafion was diluted with deionized water to a final concentration of 1 wt%. The diluted Nafion solution was printed on top of the sensing area to complete the preparation.

4.4. Preparation of labeled enzyme solution

First, 0.5 mL (1 mg) of the conjugated antibody was placed into a centrifuge tube, and 150 μL of diluted FITC solution was added, and mixed quickly. Then, 0.5 mL FITC coupling buffer was added to the desalination column and centrifuged for 2 min to remove the stored buffer. The supernatant was discarded after centrifugation. The desalination column was placed into a new centrifuge tube, and the coupling product was slowly added to the resin drop by drop. After centrifugation for 6 min, the FITC-labeled antibody was collected from the solution in the centrifuge tube.

4.5. Fabrication of tough hydrogel dressing

2.48 g of AAm and 8 mg MBAA were dissolved in 20 mL of distilled water and was stirred at 45 °C for 60 min. Then 0.31 g of sodium dodecyl sulfate was added and stirred at this temperature. After 30 min, SA was added and stirred until completely dissolved. Next, 48 mg of APS was added to the mixture and stirred quickly. Afterward, the obtained mixture was poured into a mold and degassed at room temperature to

remove air bubbles. Finally, the mold was placed under ultraviolet irradiation for 30 min. Then the hydrogel was soaked in the 0.1 M $CaCl_2$ solution for 15 min to form the double-network hydrogel.

4.6. PERfECT readout system

To enhance the wearability of the CGM device, we developed a miniaturized readout system based on our previously reported PERfECT platform (Tian et al., 2022). It features a custom firmware for data handling and integrated hardware for OECT-CGM characterization, including an ADuCM355 Analog MCU, a BLE unit, a power management module, and other necessary components assembled on a printed circuit board. The system connects to the smart patch through an FPCB connector.

4.7. Animal studies

The animal work was approved by the Animal Ethics Committee of Guangzhou Medical University (GY2023-590) and conducted following relevant guidelines. Female Sprague-Dawley (SD) rats (300–350 g) were purchased from the Guangdong Medical Laboratory Animal Center and acclimatized in an approved animal facility.

Wound biomarker monitoring was conducted using an SD rat wound model. The animals were fasted for 24 h but were allowed access to water. After administering anesthesia and analgesia with 2.5 % (v/v) isoflurane, a 5-mm full-thickness wound was created on the dorsum of each SD rat using a specialized circular cutter. The sensor array patch was then applied to the wound area and secured with a hydrogel dressing. While maintaining anesthesia, a 200 mM glucose solution in DBPS (adjusted based on body weight) was administered to the rats via a syringe. Sensor readings were collected both before and after glucose administration. For continuous blood glucose monitoring experiments, sensor readings from the wearable patch were correlated with blood glucose levels obtained by collecting blood samples from the tail vein every 15 min over 4 h.

CRediT authorship contribution statement

Binbin Cui: Writing – review & editing, Writing – original draft, Visualization, Validation, Methodology, Investigation. **Ivo Pang:** Validation, Methodology, Investigation. **Shilei Dai:** Writing – review & editing. **Xiaonan Chen:** Methodology, Investigation. **Dingyao Liu:** Methodology, Investigation. **Xinyu Tian:** Methodology. **Wensheng Lin:** Methodology, Investigation. **Jing Bai:** Investigation. **Xinran Zhang:** Investigation. **Shiming Zhang:** Writing – original draft, Supervision, Resources, Project administration, Funding acquisition, Conceptualization.

Declaration of competing interest

The authors have no conflicts of interest to declare that are relevant to the content of this article.

Acknowledgement

S.Z. acknowledges the Collaborative Research Fund (C7005-23Y), the Early Career Scheme (ECS) (27214224) and the General Research Fund (GRF) (17208623, 17200425) from the Research Grants Council of the Hong Kong SAR Government, China; the Innovation and Technology Fund (Mainland-Hong Kong Joint Funding Scheme, MHP/053/21) from the Innovation and Technology Commission (ITC) of the Hong Kong SAR Government, China. S.D. acknowledges the Postdoctoral Fellowship Scheme (PDF2324-7S07) from the Research Grants Council of the Hong Kong SAR Government, China.

Appendix A. Supplementary data

Supplementary data to this article can be found online at https://doi.org/10.1016/j.bios.2025.118345.

Data availability

Data will be made available on request.

References

Bai, J., Liu, D., Tian, X., Wang, Y., Cui, B., Yang, Y., Dai, S., Lin, W., Zhu, J., Wang, J., 2024. Coin-sized, fully integrated, and minimally invasive continuous glucose monitoring system based on organic electrochemical transistors. Sci. Adv. 10 (16) eadl1856.

Bai, J., Liu, D., Tian, X., Zhang, S., 2022. Tissue-like organic electrochemical transistors. J. Mater. Chem. C 10 (37), 13303–13311.

Bernards, D.A., Macaya, D.J., Nikolou, M., DeFranco, J.A., Takamatsu, S., Malliaras, G. G., 2008. Enzymatic sensing with organic electrochemical transistors. J. Mater. Chem. 18 (1), 116–120.

Bihar, E., Wustoni, S., Pappa, A.M., Salama, K.N., Baran, D., Inal, S., 2018. A fully inkjet-printed disposable glucose sensor on paper. npj Flexible Electronics 2 (1), 30.

Cheng, Y., Gong, X., Yang, J., Zheng, G., Zheng, Y., Li, Y., Xu, Y., Nie, G., Xie, X., Chen, M., 2022. A touch-actuated glucose sensor fully integrated with microneedle array and reverse iontophoresis for diabetes monitoring. Biosens. Bioelectron. 203, 114026.

Derakhshandeh, H., Kashaf, S.S., Aghabaglou, F., Ghanavati, I.O., Tamayol, A., 2018. Smart bandages: the future of wound care. Trends Biotechnol. 36 (12), 1259–1274.

Dong, R., Guo, B., 2021. Smart wound dressings for wound healing. Nano Today 41, 101290.

Faddoul, R., Coppard, R., Berthelot, T., 2014. Inkjet printing of organic electrochemical immunosensors. In: SENSORS, 2014. IEEE, pp. 1088–1091. IEEE.

Farahani, M., Shafiee, A., 2021. Wound healing: from passive to smart dressings. Adv. Healthcare Mater. 10 (16), 2100477.

Farooqui, M.F., Shamim, A., 2016. Low cost inkjet printed smart bandage for wireless monitoring of chronic wounds. Sci. Rep. 6 (1), 28949.

Hattori, Y., Falgout, L., Lee, W., Jung, S.Y., Poon, E., Lee, J.W., Na, I., Geisler, A., Sadhwani, D., Zhang, Y., 2014. Multifunctional skin-like electronics for quantitative, clinical monitoring of cutaneous wound healing. Adv. Healthcare Mater. 3 (10), 1597–1607.

Heck, I., Lu, W., Wang, Z., Zhang, X., Adak, T., Cu, T., Crumley, C., Zhang, Y., Wang, X.S., 2023. Soft, wireless pressure-sensor-integrated smart bandage for the management of diabetic foot ulcers. Adv. Mater. Technol. 8 (3), 2200821.

Ji, X., Lau, H.Y., Ren, X., Peng, B., Zhai, P., Feng, S.P., Chan, P.K., 2016. Highly sensitive metabolite biosensor based on organic electrochemical transistor integrated with microfluidic channel and poly (N-vinyl-2-pyrrolidone)-capped platinum nanoparticles. Adv. Mater. Technol. 1 (5), 1600042.

Kayser, L.V., Lipomi, D.J., 2019. Stretchable conductive polymers and composites based on PEDOT and PEDOT: PSS. Adv. Mater. 31 (10), 1806133.

Li, Y., Wang, N., Yang, A., Ling, H., Yan, F., 2019. Biomimicking stretchable organic electrochemical transistor. Adv. Electron. Mater. 5 (10), 1900566.

Liang, Y., He, J., Guo, B., 2021. Functional hydrogels as wound dressing to enhance wound healing. ACS Nano 15 (8), 12687–12722.

Lim, H.-R., Hillman, N., Kwon, Y.-T., Kim, Y.-S., Choa, Y.-H., Yeo, W.-H., 2020. Ultrathin, long-term stable, solid-state reference electrode enabled by enhanced interfacial adhesion and conformal coating of AgCl. Sensor. Actuator. B Chem. 309, 127761.

Liu, D., Tian, X., Bai, J., Wang, Y., Cheng, Y., Ning, W., Chan, P.K., Wu, K., Sun, J., Zhang, S., 2022a. Intrinsically stretchable organic electrochemical transistors with rigid-device-benchmarkable performance. Adv. Sci. 9 (29), 2203418.

Liu, Dingyao, et al., 2025. Increasing the dimensionality of transistors with hydrogels. Science 390 (6775), 824–830. https://doi.org/10.1126/science.adx4514.

Liu, H., Li, Z., Che, S., Feng, Y., Guan, L., Yang, X., Zhao, Y., Wang, J., Zvyagin, A.V., Yang, B., 2022b. A smart hydrogel patch with high transparency, adhesiveness and hemostasis for all-round treatment and glucose monitoring of diabetic foot ulcers. J. Mater. Chem. B 10 (30), 5804–5817.

Liu, Z., Song, H., Lin, G., Zhong, W., Zhang, Y., Yang, A., Liu, Y., Duan, J., Zhou, Y., Jiao, K., 2024. Wireless intelligent patch for closed-loop in Situ wound management. Adv. Sci. 11 (29), 2400451.

Luo, R., Dai, J., Zhang, J., Li, Z., 2021. Accelerated skin wound healing by electrical stimulation. Adv. Healthcare Mater. 10 (16), 2100557.

Marks, A., Griggs, S., Gasparini, N., Moser, M., 2022. Organic electrochemical transistors: an emerging technology for biosensing. Adv. Mater. Interfac. 9 (6), 2102039.

McLister, A., McHugh, J., Cundell, J., Davis, J., 2016. New developments in smart bandage technologies for wound diagnostics. Adv. Mater. 28 (27), 5732–5737.

Mirani, B., Pagan, E., Currie, B., Siddiqui, M., Hosseinzadeh, R., Mostafalu, P., Zhang, Y., Ghahary, A., Akbari, M., 2017. An advanced multifunctional hydrogel-based dressing for wound monitoring and drug delivery. Adv. Healthcare Mater. 6, 1700718.

Mostafalu, P., Lenk, W., Dokmeci, M.R., Ziaie, B., Khademhosseini, A., Sonkusale, S.R., 2015. Wireless flexible smart bandage for continuous monitoring of wound oxygenation. IEEE Transactions on biomedical circuits and systems 9 (5), 670–677.

Mostafalu, P., Tamayol, A., Rahimi, R., Ochoa, M., Khalilpour, A., Kiaee, G., Yazdi, I.K., Bagherifard, S., Dokmeci, M.R., Ziaie, B., 2018. Smart bandage for monitoring and treatment of chronic wounds. Small 14 (33), 1703509.

Oh, S.Y., Hong, S.Y., Jeong, Y.R., Yun, J., Park, H., Jin, S.W., Lee, G., Oh, J.H., Lee, H., Lee, S.-S., 2018. Skin-attachable, stretchable electrochemical sweat sensor for glucose and pH detection. ACS Appl. Mater. Interfaces 10 (16), 13729–13740.

Pappa, A.M., Ohayon, D., Giovannitti, A., Maria, I.P., Savva, A., Uguz, I., Rivnay, J., McCulloch, I., Owens, R.M., Inal, S., 2018. Direct metabolite detection with an n-type accumulation mode organic electrochemical transistor. Sci. Adv. 4 (6) eaat0911.

Paul, S., Gupta, M., Dey, K., Mahato, A.K., Bag, S., Torris, A., Gowd, E.B., Sajid, H., Addicoat, M.A., Datta, S., 2023. Hierarchical covalent organic framework-foam for multi-enzyme tandem catalysis. Chem. Sci. 14 (24), 6643–6653.

Salvo, P., Calisi, N., Melai, B., Dini, V., Paoletti, C., Lomonaco, T., Pucci, A., Di Francesco, F., Piaggesi, A., Romanelli, M., 2017. Temperature-and pH-sensitive wearable materials for monitoring foot ulcers. Int. J. Nanomed. 949–954.

Shim, N.Y., Bernards, D.A., Macaya, D.J., DeFranco, J.A., Nikolou, M., Owens, R.M., Malliaras, G.G., 2009. All-plastic electrochemical transistor for glucose sensing using a ferrocene mediator. Sensors 9 (12), 9896–9902.

Shirzaei Sani, E., Xu, C., Wang, C., Song, Y., Min, J., Tu, J., Solomon, S.A., Li, J., Banks, J. L., Armstrong, D.G., 2023. A stretchable wireless wearable bioelectronic system for multiplexed monitoring and combination treatment of infected chronic wounds. Sci. Adv. 9 (12) eadf7388.

Sun, J.-Y., Zhao, X., Illeperuma, W.R., Chaudhuri, O., Oh, K.H., Mooney, D.J., Vlassak, J. J., Suo, Z., 2012. Highly stretchable and tough hydrogels. Nature 489 (7414), 133–136.

Teichler, A., Perelaer, J., Schubert, U.S., 2013. Inkjet printing of organic electronics–comparison of deposition techniques and state-of-the-art developments. J. Mater. Chem. C 1 (10), 1910–1925.

Teymourian, H., Barfidokht, A., Wang, J., 2020. Electrochemical glucose sensors in diabetes management: an updated review (2010–2020). Chem. Soc. Rev. 49 (21), 7671–7709.

Tian, X., Liu, D., Bai, J., Chan, K.S., Ip, L.C., Chan, P.K., Zhang, S., 2022. Pushing OECTs toward wearable: development of a miniaturized analytical control unit for wireless device characterization. Anal. Chem. 94 (16), 6156–6162.

Wang, J., 2008. Electrochemical glucose biosensors. Chem. Rev. 108 (2), 814–825.

Wang, M., Yang, Y., Min, J., Song, Y., Tu, J., Mukasa, D., Ye, C., Xu, C., Heflin, N., McCune, J.S., 2022. A wearable electrochemical biosensor for the monitoring of metabolites and nutrients. Nat. Biomed. Eng. 1–11.

Yang, Y., Gao, W., 2019. Wearable and flexible electronics for continuous molecular monitoring. Chem. Soc. Rev. 48 (6), 1465–1491.

Zhang, S., Cicoira, F., 2017. Water-Enabled healing of conducting polymer films. Adv. Mater. 29 (40), 1703098.

Zhang, S., Hubis, E., Tomasello, G., Soliveri, G., Kumar, P., Cicoira, F., 2017. Patterning of stretchable organic electrochemical transistors. Chem. Mater. 29 (7), 3126–3132.

Zhang, S., Li, Y., Tomasello, G., Anthonisen, M., Li, X., Mazzeo, M., Genco, A., Grutter, P., Cicoira, F., 2019. Tuning the electromechanical properties of PEDOT: PSS films for stretchable transistors and pressure sensors. Adv. Electron. Mater. 5 (6), 1900191.